# Mechanism of DNA Recognition at a Viral Replication Origin*

**Cristian Oddo**[‡]**, Eleonora Freire**[‡]**, Lori Frappier**[§]**, and Gonzalo de Prat-Gay**[‡1]

*From the* [‡]*Instituto Leloir, Patricias Argentinas 435, 1405 Buenos Aires, Argentina and the* [§]*Department of Medical Genetics and Microbiology, University of Toronto, Ontario M5S 1A8, Canada*

Recognition of the DNA origin by the Epstein-Barr nuclear antigen 1 (EBNA1) protein is the primary event in latent-phase genome replication of the Epstein-Barr virus, a model for replication initiation in eukaryotes. We carried out an extensive thermodynamic and kinetic characterization of the binding mechanism of the DNA binding domain of EBNA1, $EBNA1_{452-641}$, to a DNA fragment containing a single specific origin site. The interaction displays a binding energy of 12.7 kcal mol$^{-1}$, with 11.9 kcal mol$^{-1}$ coming from the enthalpic change with a minimal entropic contribution. Formation of the $EBNA1_{452-641}$·DNA complex is accompanied by a heat capacity change of $-1.22$ kcal mol$^{-1}$ K$^{-1}$, a very large value considering the surface area buried, which we assign to an unusually apolar protein-DNA interface. Kinetic dissociation experiments, including fluorescence anisotropy and a continuous native electrophoretic mobility shift assay, confirmed that two EBNA1·DNA complex conformers are in slow equilibrium; one dissociates slowly ($t_{1/2} \sim 41$ min) through an undissociated intermediate species and the other corresponds to a fast two-step dissociation route ($t_{1/2} \sim 0.8$ min). In line with this, at least two parallel association events from two populations of protein conformers are observed, with on-rates of $0.25-1.6 \times 10^8$ M$^{-1}$ s$^{-1}$, which occur differentially either in excess protein or DNA molecules. Both parallel complexes undergo subsequent first-order rearrangements of $\sim 2.0$ s$^{-1}$ to yield two consolidated complexes. These parallel association and dissociation routes likely allow additional flexible regulatory events for site recognition depending on site availability according to nucleus environmental conditions, which may lock a final recognition event, dissociate and re-bind, or slide along the DNA.

Initiation of DNA replication from cellular and viral origins rely on origin binding proteins (OBPs),[2] also referred to as initiator proteins. These OBPs nucleate the replication machinery by recruiting various proteins and induce the local distortion of the DNA as a previous step for unwinding. There are two groups of viral OBPs, one of them is represented by the Epstein-Barr nuclear antigen 1 (EBNA1) and by the E2 protein from papillomaviruses, both of which bind to the origin but rely on other factors to melt the DNA (1). The second group consists of viral OBPs that have both DNA binding activity and helicase activity, represented by the SV-40 T antigen and the E1 helicase from papillomavirus. The second group of OBPs facilitates the binding and cooperates with those of the first group, such as the case of papillomavirus E2 that cooperates with the E1 helicase (1).

EBNA1 is the only protein expressed in all types of EBV latent infection (2). It binds to the EBV replication origin oriP where it plays several roles: initiation of DNA replication, segregation of EBV episomes, and transactivation of latent viral gene expression (3–5). All these functions require the binding of the EBNA1 DNA binding domain to specific 18-bp DNA recognition sites (6, 7). The crystal structure of this domain revealed a particular fold, the dimeric $\beta$-barrel, only shared with the papillomavirus E2 DNA binding domain (see Fig. 1) (8, 9). There is no amino acid sequence homology between these two proteins, and they belong to evolutionary unrelated virus families. Comparison of the crystal structures of the DNA-complexed forms suggested a quite different DNA binding recognition mode (10).

The portion of the EBNA1 DNA binding and dimerization domain that resembles the E2 DNA binding domain from papillomavirus is referred to as the core domain (residues 504–604). This includes the dimeric barrel interface and two $\alpha$-helices, one of which is the recognition helix. A noticeable difference in the core domain is the length and position of a loop connecting $\beta$-strands 2 and 3. In EBNA1, this loop contains nine extra residues, five of which are proline residues, and is therefore termed the proline loop. Although the helix corresponding to the recognition helix in E2 domain is present in the EBNA1, it is located 6 Å away from the DNA. However, mutagenesis of this helix and the fact that the core alone binds DNA suggest a role of this helix in DNA binding (11). The EBNA1 flanking domain (Fig. 1) is composed of an extended chain (461–476) that tunnels through the minor groove of the $\alpha$-helix (477–489), and a connector (490–503) linking this domain with the core domain. An acidic tail is located at the C terminus of the protein (608–641). Neither acidic nor flanking domains or equivalent domains are present in papillomavirus E2 C-terminal domains. The Epstein-Barr genome includes repetitive contiguous EBNA1 binding elements, and assembly at these sites is cooperative, where the DNA binding domain alone is sufficient for cooperative binding (12). Changes in the

---

[1] A Career Investigator from Consejo Nacional de Investigaciones Científicas y Técnicas. To whom correspondence should be addressed. Tel.: 54-011-5238-7500; Fax: 54-011-5238-7501; E-mail: gpratgay@leloir.org.ar.

[2] The abbreviations used are: OBP, origin binding protein; EBNA1, Epstein-Barr nuclear antigen 1; EBV, Epstein-Barr virus; Bis-Tris, 2-[bis(2-hydroxyethyl)amino]-2-(hydroxymethyl)propane-1,3-diol; EMSA, electrophoretic mobility shift assay; ITC, isothermal titration calorimetry; HPV, human papillomavirus.
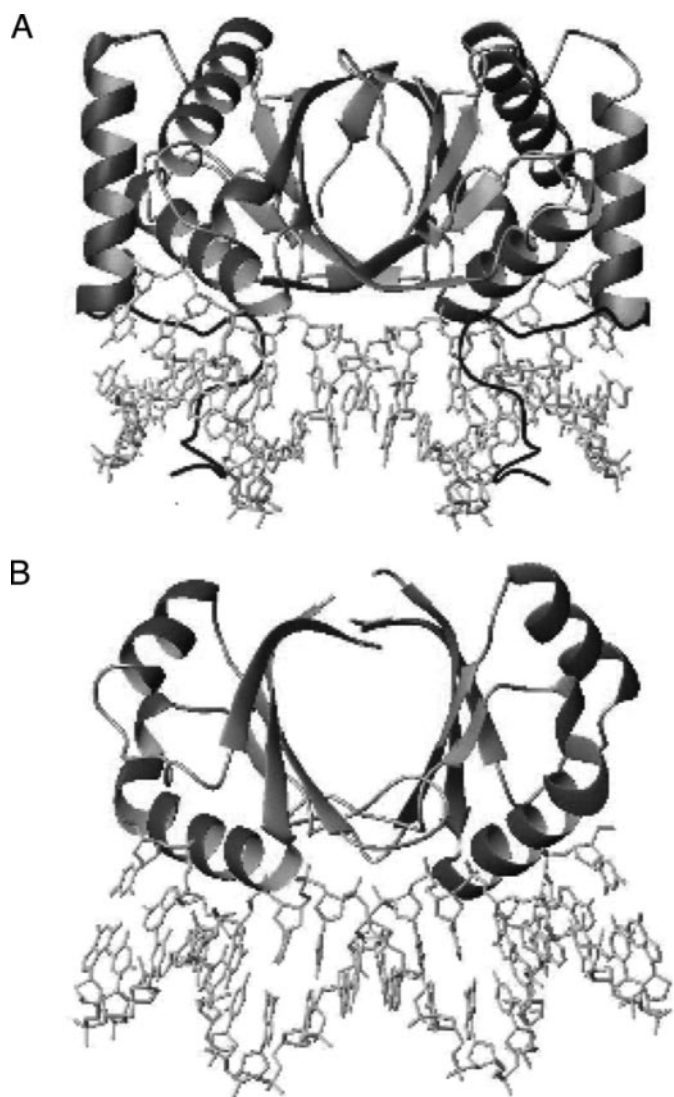
FIGURE 1. **Structure of the EBNA1 DNA binding domain.** *A*, schematic representation of the crystal structure of Epstein-Barr EBNA1 binding and dimerization domain bound to an EBNA1 recognition site (PDB code 1B3T) (10). *B*, schematic representation of the HPV-18 E2C binding and dimerization domain bound to an E2 recognition site (PDB code 1BOP) (34).

DNA, including bending, take place upon binding (10), which result in permanganate sensitivity (13), and DNA unwinding is predicted to accompany assembly of EBNA1 on two adjacent sites (10).

We have been investigating the DNA binding mechanisms of the E2 DNA binding domain from human papillomavirus (14–16) and our goal is to compare the only two dimeric β-barrel domains described so far that incidentally bind at or near DNA replication origins. In the present work, we analyzed the DNA binding mechanism of EBNA1 to a single specific DNA site in solution, a model for eukaryotic replication origins, using various spectroscopic, biophysical, and calorimetric techniques. We integrated structural thermodynamic and kinetic data and compared them with the E2 DNA binding domain.

## EXPERIMENTAL PROCEDURES

*Chemicals*—All reagents were of analytical grade and purchased from ICN (Aurora, OH) or Sigma. All solutions were prepared with distilled and deionized (Milli-Q plus) water and filtered through 0.45-$\mu$M membranes prior to use.

*DNA Synthesis*—Double-stranded 20-bp oligonucleotides containing one EBNA1 recognition sequence (Site 1 of the dyad symmetry element of *oriP* in the Epstein-Barr B95-8 strain genome) were prepared as follows: single-stranded oligonucleotides were purchased, high-performance liquid chromatography-purified, from Integrated DNA Technologies (Coralville, IA): Site 1A, 5′-C*GGGAAGCATATGCTACCC*G-3′ (recognition sequence is italicized); Site 1B, 5′-6-carboxyfluorescein (FAM) is the complementary strand with a fluorescein molecule attached to the 5′-end via a 6-carbon linker. Single-stranded oligonucleotide concentration was calculated using the molar extinction coefficient at 260 nm obtained from the nucleotide composition. Annealing was performed by mixing equal amounts of the oligonucleotides in 10 mM Bis-Tris HCl buffer, pH 7.0, and 100 mM NaCl, further incubating the mixture for 5 min at 95 °C, and slowly cooling to 25 °C for 16 h. This yielded a double-stranded oligonucleotide termed Site 1 5′-FAM, and no detectable single-stranded oligonucleotide was present as judged by PAGE (not shown). A similar procedure was followed to anneal the Tesi-1-5′-FAM 5′-ATC-CCAGCCAGTGTCGAGAG-3′. This oligonucleotide corresponds to the randomized Site 1 sequence keeping the same base composition. The double-stranded E2 oligonucleotide, termed Site 35-5′-FAM and used as nonspecific DNA, was 5′-GTAACCGAAATCGGTTGA-3′.

*Protein Expression and Purification*—Recombinant full-length EBNA1 was expressed and purified from baculovirus-infected insect cells as previously described (17). The procedure is much more complex, the yields are lower, and this protein cannot be expressed in bacteria. The recombinant C-terminal domain of EBNA1 (EBNA1$_{452-641}$) was expressed in *Escherichia coli* BL21(DE3) pLys S, using a modified protocol from the one previously described (18, 19). Bacterial cells expressing EBNA1$_{452-641}$ were grown in a 1.5-liter fermenter (New Brunswick Scientific Co., Inc, Edison, NJ) in Terrific Broth culture medium at 37 °C, to an absorbance of 5 at 600 nm. EBNA1$_{452-641}$ expression was induced with 0.5 mM isopropyl β-D-thiogalactopyranoside, followed by the addition of 150 $\mu$g/ml rifampicin 3 h later. The cells were incubated overnight, harvested by centrifugation, and resuspended in 0.1 volume of the lysis buffer (100 mM Tris HCl, pH 6.8, 600 mM NaCl, 1.0 mM EDTA, 1.0 mM phenylmethylsulfonyl fluoride, and 10 mM 2-mercaptoethanol). Cells were frozen at −70 °C and then thawed at room temperature, and subsequently lysed by sonication at 0 °C twice. The lysate was clarified by centrifugation at 20,000 × *g* for 20 min. The supernatant was then placed in a 75 °C water bath until the temperature of the protein solution reached the temperature of the bath. Heating was followed by a 10-min incubation on ice. The supernatant was clarified by centrifugation at 20,000 × *g* for 40 min and then loaded onto a heparin HyperD (BioSepra, Villeneuve la Garenne, France) affinity column equilibrated with buffer A (50 mM Tris-HCl, pH 7.2, 0.2 M NaCl, and 5 mM 2-mercaptoethanol), washed with 5 column volumes of the same buffer, and eluted with 0.15–1.0 M NaCl linear gradient. The fractions that were over 90% pure were pooled, dialyzed against buffer A without 2-mercaptoeth-

anol, and digested with thrombin (1.5 units/mg of protein) at 37 °C for 7 h to remove the His$_6$ tag. Digestion was stopped with 0.2 mM phenylmethylsulfonyl fluoride, and the protein was loaded onto a Mono Q ion exchange column (Amersham Biosciences), equilibrated with buffer A, and washed with 5 column volumes of the same buffer. The protein eluted in a 15-ml linear gradient from 0.2 to 1.0 M NaCl in buffer A. The fractions that were greater than 95% pure as judged by SDS-PAGE were pooled, concentrated using Centriprep-10 (Amicon, Bedford, MA), and loaded onto a Superdex 75 gel-filtration column (Amersham Biosciences). This procedure yielded around 20 mg/liter of >98% pure EBNA1$_{452-641}$. The purified protein was dialyzed against 25 mM Tris HCl, pH 7.2, 500 mM NaCl, 0.2 mM EDTA, 10% glycerol, and 5 mM 2-mercaptoethanol, and stored at ~150 $\mu$M fractions at −70 °C after snap freezing in liquid nitrogen. Protein concentration was determined using an extinction coefficient of $4.19 \times 10^4$ M$^{-1}$ cm$^{-1}$.

*DNA Binding*—Fluorescence measurements were recorded in an Aminco Bowman series 2 luminescence spectrometer assembled in "L" geometry. For fluorescein anisotropy measurements excitation was set to 495 nm with a 4 nm slit, and emission was recorded at 520 nm. When fluorescein concentration was lower than 20 nM, the excitation slit was set to 8 nm. The temperature was kept constant at 25 ± 0.1 °C through all experiments. All titrations were performed adding small amounts of a concentrated solution of the variable ligand to fixed amounts of a concentrated solution of the other and allowed to equilibrate for 2 min. In all cases, maximal dilution was 20%, and the data were corrected accordingly.

Dissociation constants for the EBNA1·DNA complex were performed in 25 mM Bis-Tris-HCl (pH 7.0), 200 mM NaCl, and 1 mM dithiothreitol by measuring the steady-state fluorescence anisotropy of the 5′-FAM·DNA as a function of added EBNA1. Data were fitted using nonlinear least squares to Equation 1,

$$[EBNA1 - DNA] = 0.5\Delta F([DNA] + [EBNA1] + K_D)$$

$$- ((([DNA] + [EBNA1] + K_D)^2 - (4[DNA][EBNA1]))^{0.5} \quad \text{(Eq. 1)}$$

where $\Delta F$ is the difference in the signal between the EBNA1·DNA complex and free DNA; [DNA] and [EBNA1] are the oligonucleotide and protein concentrations, respectively; and $K_D$ is the dissociation constant for the interaction. No computational corrections for emission intensity were required, because the quantum yield did not change significantly upon binding.

*Electrophoretic Mobility Shift Assay*—Standard equilibrium EBNA1·Site 1 binding was carried out in identical conditions to equilibrium binding by fluorescence spectroscopy (25 mM Bis-Tris-HCl pH 7.0, 0.2 M NaCl, and 1 mM dithiothreitol) at 2 $\mu$M Site 1 5′-FAM and different molar ratios of EBNA1$_{452-641}$, followed by 60-min incubation at room temperature in a final volume of 50 $\mu$l. For the EBNA1·Site 1 dissociation experiment, reaction mixtures in the same buffer containing 1 $\mu$M EBNA1$_{452-641}$·Site 1 5′-FAM complex and large excess of unmodified Site 1 were incubated 60 min at room temperature in a final volume of 15 $\mu$l. Finally, for EBNA1·Site 1 off-rate kinetics, the procedure was as follows: reaction mixtures in the same buffer containing a 5 $\mu$M EBNA1$_{452-641}$·Site 1 5′-FAM

complex were incubated 60 min at room temperature and then a 30-fold excess of unmodified Site 1 was added to a final volume of 100 $\mu$l to displace the Site 1 5′-FAM from the complex. Mixtures were loaded continuously into running 10% non-denaturing polyacrylamide gels containing TBE (0.1 M Tris-HCl, pH 8.0, 0.15 M sodium borate, 4 mM EDTA) 0.5×. The gels were resolved at 4 V/cm, 4–8 °C for 2–8 h. Fluorescein bands were detected by UV transillumination. After visualization and documentation, the gels were silver stained.

*Circular Dichroism*—CD spectra were monitored in the near UV region using Jasco J-810 equipment. Ten scans were averaged for each measurement at 25.0 ± 0.1 °C controlled by a peltier, and contribution of the protein was subtracted. It is expected that in the 250 to 320 nm range, the ellipticity of the protein does not change substantially (*i.e.* the contribution is linear), and thus we can assume we are evaluating mainly changes in DNA conformation (20).

*Isothermal Titration Calorimetry*—All experiments were conducted using a VP ITC (MicroCal Inc., Northampton, MA). Titrations were performed as described elsewhere (21, 22). In a typical experiment, 8-$\mu$l injections of EBNA1$_{452-641}$ were made into DNA solution in the cell. The heat of dilution of the protein into the buffer was determined in separate experiments and subtracted from the titration prior to data analysis. The data were analyzed using the ORIGIN software supplied with the calorimeter. The dissociation binding constants in the temperature range of 293–308 K were too high to be determined from the ITC results, because of the high concentrations of protein that were required to detect the heats of binding and the tight binding involved.

*Stopped-flow Kinetics*—All fluorescence stopped-flow kinetic experiments were performed using an SX.18MV stopped-flow apparatus (Applied Photophysics, Leatherhead, UK). Concentrations reported are those resulting from mixing equal volumes of each syringe at 25 ± 0.1 °C, unless otherwise stated. The reactions were monitored using the fluorescence of the 5′-FAM moiety of the modified oligonucleotides or the intrinsic Trp fluorescence of the protein. Excitation was set to 490 nm or 280 nm and the total fluorescence recorded through cut-off filters (Schott, PA). Five to ten kinetics traces were collected and averaged for each concentration point. The data were analyzed to extract the rates and amplitudes using non-linear least squares fitting software provided by the manufacturer, using single or double exponential equations. The errors for the constants were between 2 and 10%. The Double-jump association-dissociation experiments were performed mixing 0.5:0.5 volumes of protein and 5′-FAM·DNA, and, after the "delay time," the reaction sample was subsequently mixed with one volume of non-fluoresceinated DNA, and the fluorescent decay was measured.

## RESULTS

*Binding of EBNA1$_{452-641}$ at the Equilibrium*—To determine the stoichiometry in solution we carried out binding titration experiments at concentrations well above the expected dissociation constant. We used fluorescein modified or unmodified 20-bp duplexes corresponding to the specific Site 1 of the dyad symmetry element of EBV oriP (7), and the buffer conditions were optimized for minimizing aggregation and additives (see
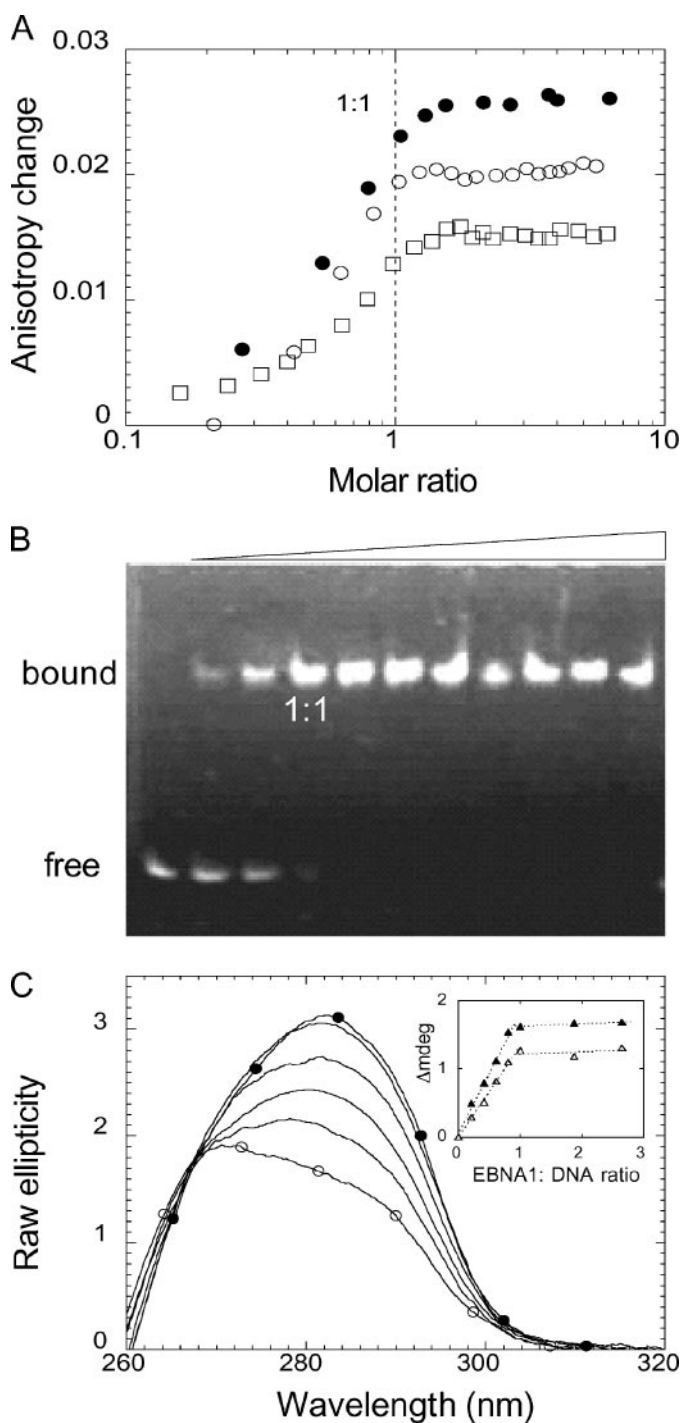
FIGURE 2. **Stoichiometry of the EBNA1$_{452-641}$-DNA interaction.** *A,* titration curves of the Site 1 5′-FAM at 20 nM (□), 200 nM (●), and 500 nM (○) with increasing amounts of EBNA1$_{452-641}$ monitored by fluorescein fluorescence anisotropy. *B,* native gel electrophoresis of EBNA1$_{452-641}$-Site 1 interaction. Site 1 5′-FAM oligonucleotide was incubated at 2 $\mu$M with different molar ratios of EBNA1 and subjected to native polyacrylamide gel electrophoresis. Silver staining of the gel confirms that all shifted bands contain protein (not shown). *C,* DNA conformational changes induced by EBNA1 binding analyzed by a stoichiometric titration. Site 1 was incubated at 2 $\mu$M with different concentrations of EBNA1$_{452-641}$, free DNA (○), and 2 $\mu$M EBNA1$_{452-641}$ (●). CD spectra were recorded (*inset,* same titration showing the ellipticity change at 270 nm (△) and 292 nm (▲)).

"Experimental Procedures"). Fluorescence intensity and anisotropy were measured upon addition of pure recombinant EBNA1$_{452-641}$ and revealed a 1:1 stoichiometry (Fig. 2*A*). We

wanted to confirm the stoichiometry by different techniques, because we had to either rule out or consider nonspecific or low affinity binding events in solution. The related HPV E2C DNA binding domain showed additional binding events in solution, not observed in previous assays or x-ray structures (14, 23). Gel-filtration experiments show that, even in a large excess of protein, the complex formed has the expected size of a 1:1 EBNA1·Site 1 globular complex (not shown).

We carried out an EMSA experiment at similar concentrations to those in the binding titration and confirmed a 1:1 stoichiometry, either in excess of protein (Fig. 2*B*) or DNA (not shown). This differs from what was observed in E2C in identical conditions used as control in this experiment (not shown) (14). It agrees with the stoichiometry observed in previous EMSA assays using radioactive detection, carried out at much lower concentrations (11).

As a probe for the binding from the DNA end, we used near-UV CD, which allows discrimination of changes exclusively taking place on the DNA. Upon addition of EBNA1$_{452-641}$ to an unmodified Site 1 duplex, there was a change in the spectra, indicative of a substantial change on its conformation upon binding of the domain (Fig. 2*C*). An increase in the bands at ~280 nm could be indicative of DNA unwinding, but because the contributions in this region are so complex, it is virtually impossible to assign a particular structure (20). The *inset* of the figure shows that the stoichiometry was also 1:1, as judged by the ellipticity change in the DNA followed at two different wavelengths (Fig. 2*C, inset*).

To determine the dissociation constant, we carried out binding isotherms under near dissociation conditions, following fluorescein anisotropy at different DNA and protein concentrations (Fig. 3*A*). The data were fitted to a quadratic binding equation, and the residuals are indicated in the *inset*. The $K_D$ was determined to be 0.5 ± 0.1 nM, in excellent agreement with previous EMSA results (11). Using the same procedure, the binding of a nonspecific sequence with the same base content yield as the specific E2 site showed a $K_D > 10$ $\mu$M (Fig. 3, *inset*), and the discrimination capacity ($K_{D\text{non-specific}}/K_{D\text{specific}}$) is at least 20,000, in the same range of what was observed for HPV16 E2C (14).

As a test for the biological relevance of studying the DNA binding domain rather than the difficult to express full-length form, we determined the dissociation constant of the baculovirus-expressed EBNA1 (see "Experimental Procedures") for comparison. We carried out the comparison in 400 mM NaCl in the same buffer, because it weakens the extremely tight interaction, and allows an accurate determination with the best signal-to-noise ratio possible. In these conditions, the $K_D$ of EBNA1 was 1.0 ± 0.1 nM, compared with 1.2 ± 0.2 nM for the EBNA1$_{452-641}$ domain to the same DNA site, which validates our analysis.

*Thermodynamics of EBNA1$_{452-641}$-DNA Binding*—To evaluate the thermodynamic parameters governing the interaction of EBNA1$_{452-641}$ with its specific DNA site, we carried out ITC experiments. Upon addition of EBNA1$_{452-641}$ to a solution containing the EBNA1 Site 1 duplex, a strong enthalpic change was observed, where the raw data indicated a tight and saturable interaction, as expected (Fig. 4*A*). The data were fitted to a
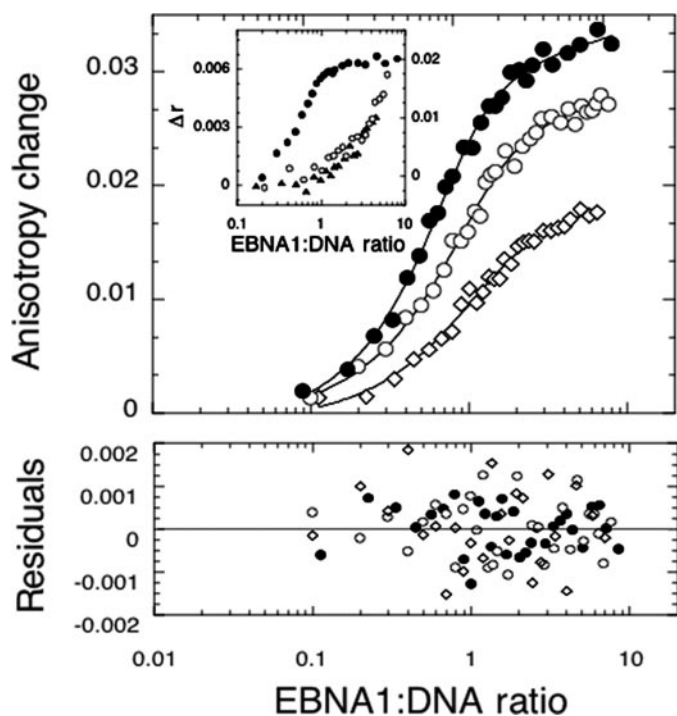
FIGURE 3. **Equilibrium dissociation constant measurement.** Binding experiments were performed by adding EBNA1$_{452-641}$ to a fixed amount of oligonucleotide Site 1 5'-FAM and monitored by the fluorescein fluorescence anisotropy. High affinity binding was carried out at the following fixed concentrations: 1.0 nM ($\diamond$), 2.0 nM ($\bigcirc$), and 5.0 nM ($\bullet$). *Inset*, low affinity binding comparison of nonspecific fluoresceinated oligonucleotides with Site 1 5'-FAM. The *left axis* corresponds to 500 nM Tesi1 (Site 1 random sequence) ($\bigcirc$) and 500 nM HPV18 Site 35 ($\blacktriangle$). The *right axis* corresponds to 5.0 nM Site 1 5'-FAM ($\bullet$). The *lower panel* shows residuals for the fittings to Equation 1. The calculated $K_D$ was 0.5 ± 0.1 nM.



FIGURE 4. **Isothermal titration calorimetry.** *A*, binding isotherm for the titration of EBNA1$_{452-641}$ (121 $\mu$M) to a solution containing Site 1 DNA (10.5 $\mu$M) at 298 K in 25 mM Bis-Tris-HCl (pH 7.0) buffer, 200 mM NaCl, 0.1 mM dithiothreitol. The data were analyzed to obtain estimates of $n$, $\Delta H_{obs}$, $\Delta S$, and $K_{obs}$ and their uncertainties using the "single set of identical sites" model within the Origin software package. The fit line yielded a stoichiometry of 0.87 ± 0.01, a binding enthalpy of −11.9 ± 0.14 kcal/mol, and entropy of −8.55 × 10$^{-3}$ kcal mol$^{-1}$ K$^{-1}$. The $K_D$ was not reliable at these experimental conditions. *Inset*, raw ITC data from the titration shown in *panel A*. *B*, $\Delta H_{obs}$ *versus* temperature for EBNA1·DNA ($\bullet$) and E2C·DNA interaction ($\bigcirc$) (29). The *line* represents the linear least-squares regression to the experimental data.

standard binding equation, showing a 1:1 stoichiometry, and the dissociation could not be determined accurately, due to the limits imposed by the technique. The $K_D$ used was that determined from fluorescence titration experiments: $0.5 \times 10^{-9} \pm 0.1 \times 10^{-9}$ M (free energy for the binding process $\Delta G = -12.7 \pm 0.1$ kcal mol$^{-1}$); the $\Delta H_{obs}$ was $-11.9 \pm 0.14$ kcal mol$^{-1}$ (Fig. 4*A*). Using these data, the entropic change, $\Delta S$ was calculated to be only $+2.7 \pm 0.9$ cal mol$^{-1}$ K$^{-1}$, indicating that the interaction is, to a great extent, enthalpically driven.

Formation of protein·DNA complexes is accompanied by a heat capacity change ($\Delta C_p$), which is related to the amount of hydration of the polar or apolar molecular surfaces (24). ITC experiments were carried out at different temperatures, and the $\Delta H_{obs}$ was plotted against the temperature, and the slope corresponds to the $\Delta C_p$ of the interaction. The formation of the EBNA1·DNA complex was accompanied by a $\Delta C_p$ of $-1.22 \pm 0.08$ kcal mol$^{-1}$ K$^{-1}$.

*Kinetic Dissociation of EBNA1$_{452-641}$·DNA*—To determine the overall binding mechanism, we started analyzing the kinetic dissociation of EBNA1$_{452-641}$ to DNA. For this, we incubated an EBNA1$_{452-641}$·5'-FAM Site 1 complex with an excess of unmodified EBNA1 Site 1 DNA duplex, and determined the anisotropy change after 4 h. A 25-fold excess of unmodified DNA ensures dissociation of the complex as the anisotropy change indicated (not shown). The formation of the complex was very fast as the change in anisotropy of the 5'-FAM Site 1 was immediately increased upon addition of EBNA1$_{452-641}$
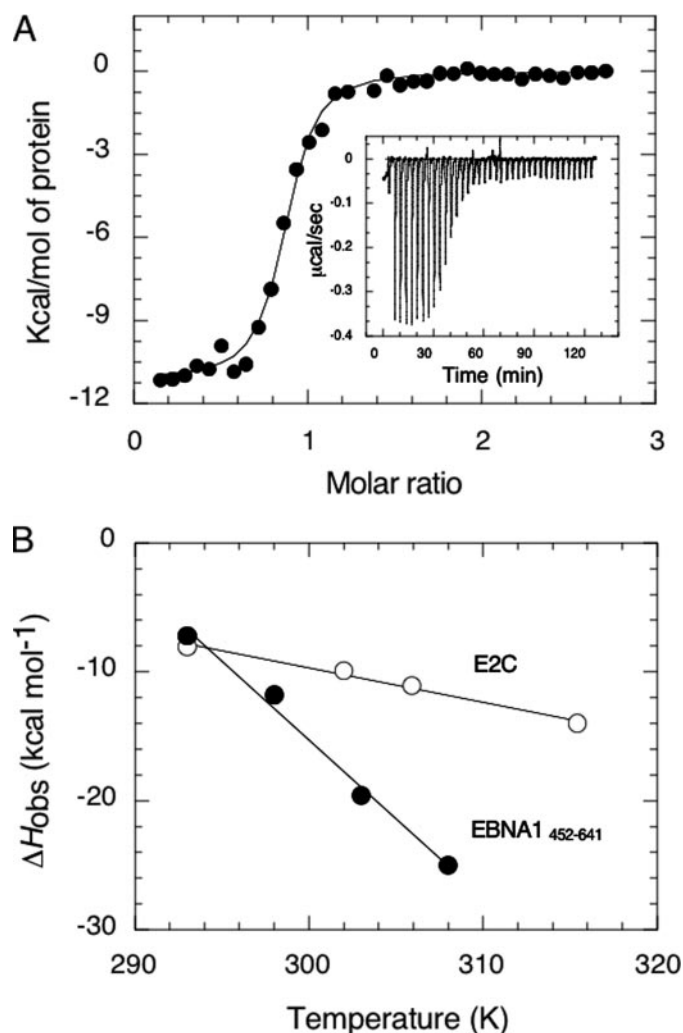
protein (not shown). After a 30-min stabilization period, addition of a 25-fold excess of unmodified Site 1 DNA decreased the anisotropy, as expected for the dissociation (Fig. 5*A*). The anisotropy change that accompanies dissociation was fitted to two exponential phases, and the residuals are indicated (Fig. 5*A*, *bottom panel*). The phases contribute each with 50% of the amplitude, and the first order rates were $2.8 \times 10^{-4}$ s$^{-1}$ for $k^r_{-3}$, and $2.7 \times 10^{-3}$ s$^{-1}$ for $k^r_{-2}$, corresponding to $t_{1/2}$ values of 41 and 4.3 min, respectively. A similar experiment was carried out in the stopped-flow equipment monitoring fluorescence intensity. The advantage of this technique is that faster reactions can be observed, but there is a limitation for slow reactions that can be observed in a standard fluorometer. Fig. 5*B* shows the data in the 0- to 1000-s range where a fast phase corresponding to 20% of the amplitude and a $k^{FAM}_{-1}$ rate of 0.011 s$^{-1}$ was observed, and a slower phase with a rate of 0.001 s$^{-1}$ was observed, which
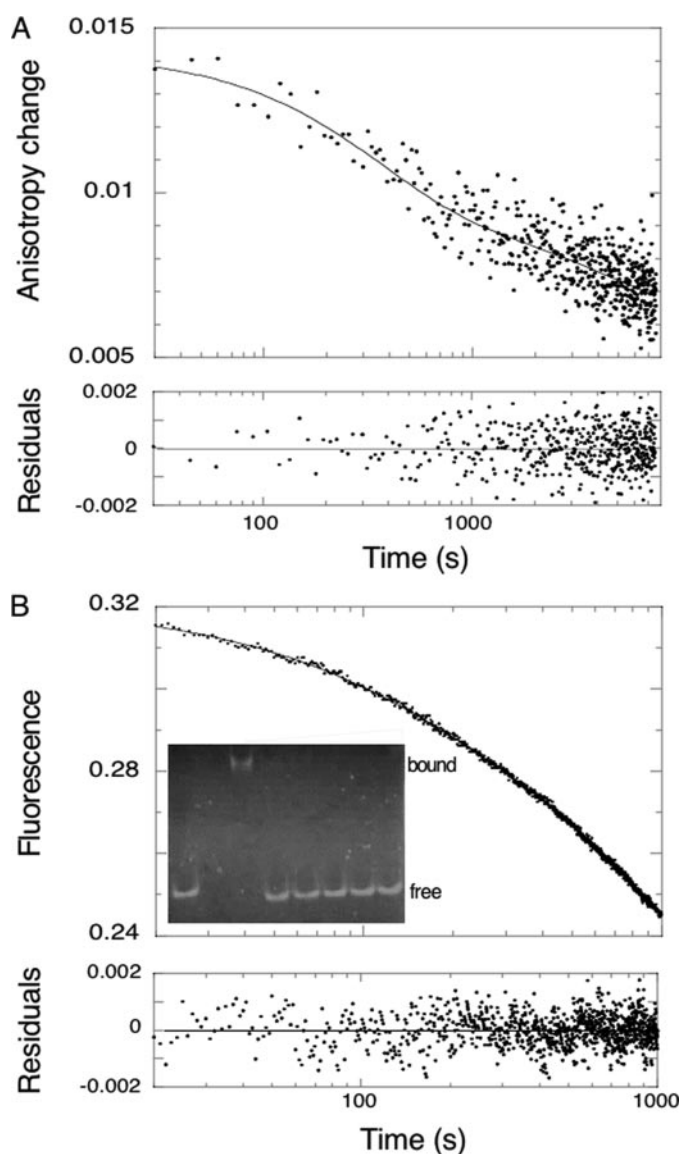
FIGURE 5. **Dissociation kinetics of EBNA1 from Site 1 DNA.** *A,* equimolar complex between 200 nM Site 1 5-FAM and 200 nM EBNA1$_{452-641}$ was incubated for 30 min and out-competed with a 25-fold molar excess of unlabeled Site 1. Fluorescence anisotropy of the 5′-FAM was recorded. The *line* represents the best fit of the data points to the anisotropy changes. The *lower panel* shows residuals for the fitting to double exponential. *B,* equimolar complex between 100 nM Site 1 5-FAM and 100 nM EBNA1$_{452-641}$ was incubated for 30 min and out-competed with a 25-fold molar excess of unlabeled Site 1. A stopped-flow trace of the 5′-FAM fluorescence was recorded. The *line* represents the best fit of the data points to the fluorescence changes. *Inset,* EBNA1$_{452-641}$·Site 1 5′-FAM 1 μM complex dissociation followed by native EMSA. Complexes were incubated 1 h at room temperature with different molar excess of Site 1 and subjected to native polyacrylamide gel electrophoresis. Silver staining of the gel confirms that all shifted bands contain protein (not shown). The *lower panel* shows residuals for the fitting to double exponential.
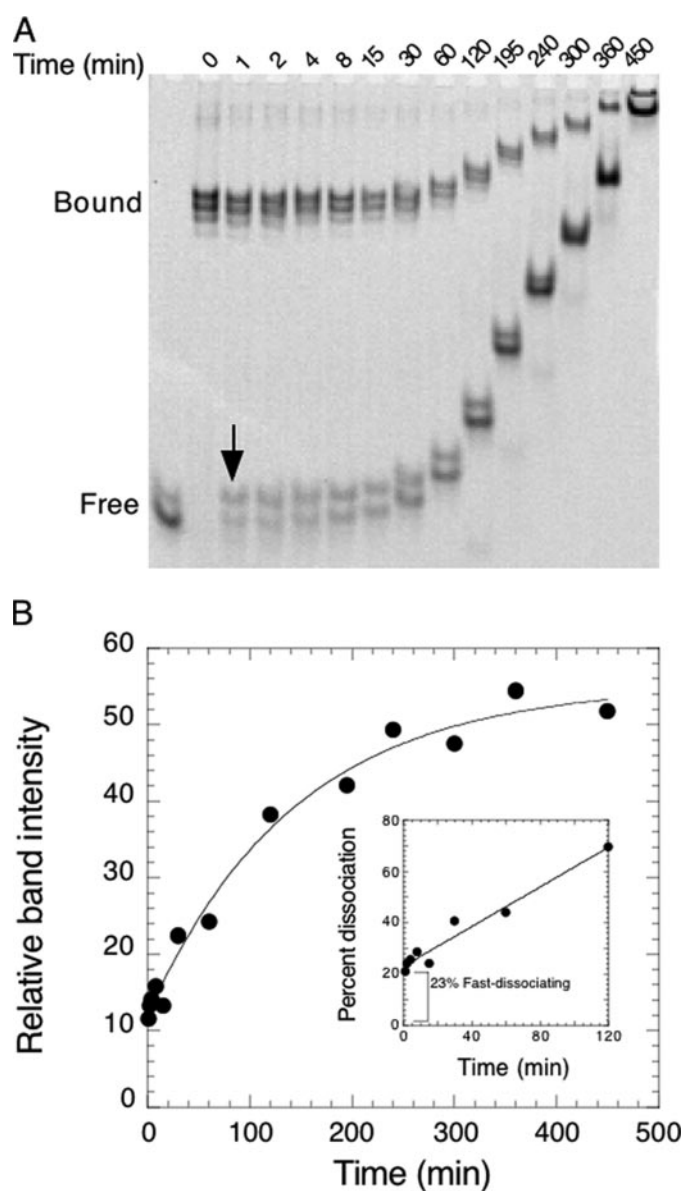


FIGURE 6. **Kinetic dissociation of EBNA1·Site 1 complex followed by a continuous EMSA assay.** Fluoresceinated Site 1 oligonucleotide was incubated with EBNA1$_{452-641}$ as described under "Experimental Procedures." The decay of the fluoresceinated complexes was analyzed as a function of time on a continuously run polyacrylamide gel, following the addition of a vast excess of non-fluoresceinated competitor. *A,* direct visualization of the fluorescein label in the entire time course for a typical experiment. The elapsed time in minutes is shown *above* each *lane.* *B,* quantification of the fluorescence-free DNA band using the ImageQuaNT 5.2 package software. The *line* represents the best fit of the data points to single exponential decay that yields a dissociation rate constant of 0.0069 ± 0.0011 min$^{-1}$. *Inset,* the percent dissociation was calculated and the initial segment of the single exponential approached to a linear function. The evident non-zero interception indicates that 23% of the population corresponds to fast dissociating protein·DNA complexes.

we assigned by coincidence to the $k^r_{-2}$ from anisotropy (Fig. 5*A*). We confirmed the complete dissociation of the DNA by an EMSA experiment. The EBNA1$_{452-641}$·5′-FAM Site 1 complex (Fig. 5*B, inset, lane 3*) was displaced into the free 5′-FAM Site 1 by excess unmodified Site 1 DNA (Fig. 5*B, inset, lanes 4 – 8*).

Finally, to assign the observed constants ($k^r_{-3}$ and $k^r_{-2}$) within the overall dissociation reaction by a direct measurement, we followed the displacement of the EBNA1$_{452-641}$·5′-FAM Site 1

complex by a continuous EMSA assay. After complex formation, the same excess of unfluoresceinated Site 1 DNA duplex as in the anisotropy experiments was added (Fig. 5), and at the indicated times aliquots were withdrawn and loaded into a continuously running native gel. Fig. 6*A* shows the gradual increase of free 5′-FAM Site 1 DNA, a product of the dissociation of the complex increasing with elapsed time. The integrated bands were plotted against time, and the data were fitted to a single

exponential equation, yielding a $t_{1/2}$ of ~100 min, in very good agreement with the anisotropy experiment (41 min), considering the large difference in the accuracy of the experiments (Fig. 6*B*).

Analysis of the early points indicates that they do not extrapolate to zero. The initial portion of an exponential reaction can be approached to a linear function and such analysis is shown in the *inset* of Fig. 6*B* (25). The non-zero extrapolation within the dead time of the experiment indicates that $23 \pm 2\%$ of the population of the complex effectively dissociated very rapidly (see *arrow* in Fig. 6, *A* and *B*). The fast rate observed from stopped-flow dissociation experiments monitored by fluorescence intensity (0.011 s$^{-1}$, Fig. 5*B*) is compatible with this phase.

*Two-step Association-Rearrangement Mechanism*—The association kinetics was investigated by a pseudo first order experiment, where a fixed concentration of 5′-FAM Site 1 DNA oligonucleotide was mixed with increasing concentrations of EBNA1$_{452-641}$ in a stopped-flow fluorometer. There was a fast fluorescence increase involving at least two phases, as the data fit to two exponential components (Fig. 7*A*, and *insets*). The observed pseudo first order rates were plotted against protein concentration, and the data are shown in Fig. 7*B*. The major phase ($k_1$, Fig. 7*B*), accounting for 85% of the amplitude, is concentration-dependent and thus corresponds to the association event, with a $k_{on1}^{FAM}$ of $1.6 \times 10^8$ M$^{-1}$ s$^{-1}$, in the range of a diffusion controlled reaction. The minor phase, accounting for 15% of the amplitude, did not depend on the concentration, indicating that it corresponds to a conformational rearrangement, most likely after the collision event, with a first order rate of 2.0 s$^{-1}$ ($k_2$, Fig. 7*B*). The extrapolation to zero protein provides an estimate of the $k_{off}$, but it was only possible to confirm it as $\leq 0.5$ s$^{-1}$.

We carried out a similar stopped-flow experiment in pseudo-first order conditions but following the change in the intrinsic tryptophan fluorescence of EBNA1$_{452-641}$ upon binding to DNA. In this experiment two binding events were observed: a major phase ($k_1$, Fig. 7*C*) accounting for 85% of the amplitude was also observed with a $k_{on1}^{W}$ of $1.0 \times 10^8$ M$^{-1}$ s$^{-1}$, confirming the association rate with a different probe (Fig. 7*C*). A minor phase ($k_3$, Fig. 7*C*) corresponding to 15% of the amplitude and a second-order rate $k_{on2}^{W}$ of $0.25 \times 10^8$ M$^{-1}$ s$^{-1}$ indicated two parallel binding events. The sensitivity of tryptophan fluorescence was comparatively much lower than the 5′-FAM fluorescence, so we were not able to measure the minor phase as accurately. In any case, the minor phase was slightly but significantly lower.

*Double-jump Experiments*—A double-jump association-dissociation experiment consists of mixing EBNA1$_{452-641}$ protein with 5′-FAM Site 1 DNA, allowing the binding reaction to proceed, and at different "delay" times ranging from 0.01 to 100 s, it dissociates the complex with an excess of unmodified Site 1 DNA and monitors the fluorescence change accompanying the dissociation. When the complex was formed in excess of protein (800 nM protein: 100 nM 5′-FAM DNA), and displaced with excess of unlabeled DNA, a single phase was observed in a 200-s time frame with a rate of 0.014 s$^{-1}$ ($k_{-1}^{DJ}$, Fig. 8*C*), coincident with the faster rate observed for dissociation of the complex followed by stopped flow ($k_{-1}^{FAM}$, Fig. 5*C*). Under these experi-
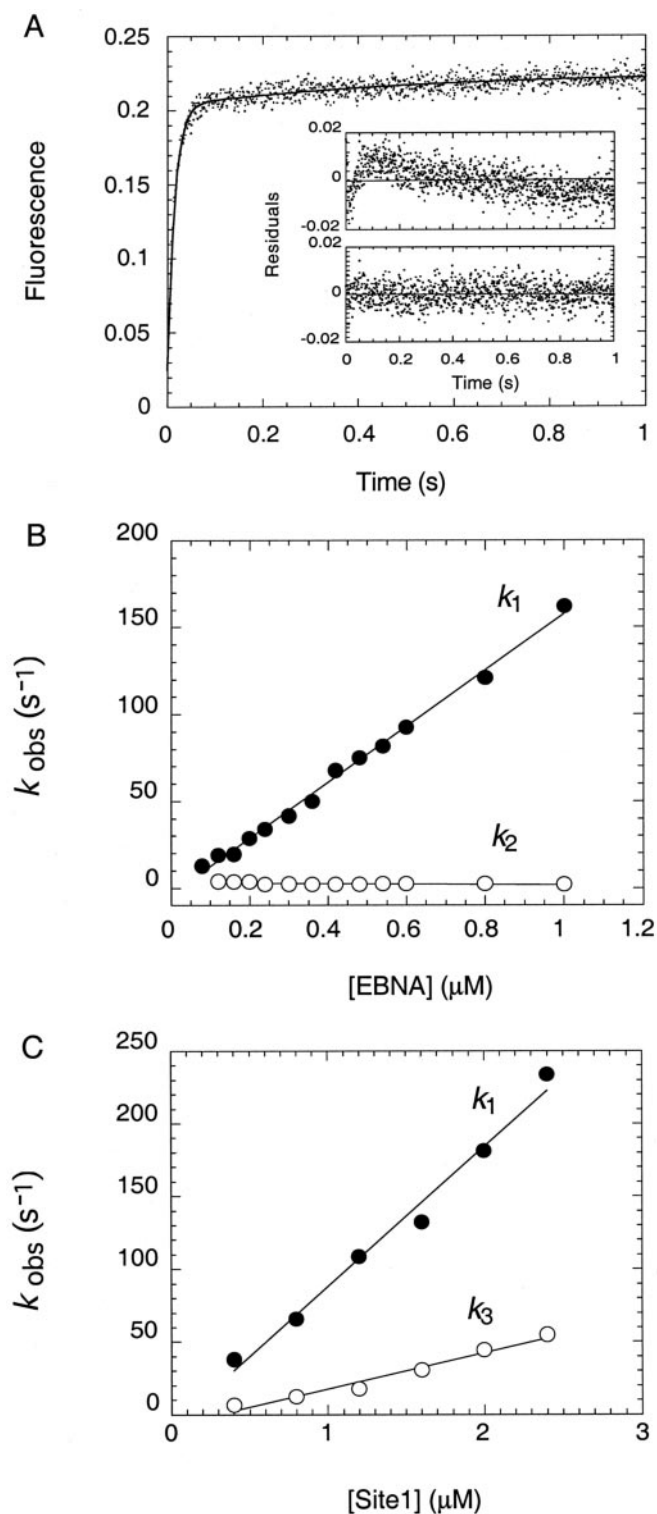


FIGURE 7. **Kinetic association of EBNA1 domain to DNA under pseudo-first order conditions.** *A*, typical stopped-flow fluorescence trace at 20 nM Site 1 5′-FAM and 100 nM EBNA1$_{452-641}$. The *line* represents the best fit of the data points to the fluorescence changes (the *top* and *bottom* insets show residuals to single and double exponentials, respectively). *B*, pseudo-first order plot for the association between 20 nM oligo Site 1 5′-FAM with different concentrations of EBNA1$_{452-641}$. The 5′-FAM fluorescence change was recorded, and the data were fitted to a double exponential process: $k_{on1}^{FAM}$ (●) and $k_2$ (○). *C*, pseudo-first order plot for the association between 100 mM EBNA1$_{452-641}$ with different concentrations of Site 1. The Trp fluorescence change was recorded, and the data were fitted to a double exponential process: $k_{on1}^{w}$ (●) and $k_{on2}^{w}$ (○).
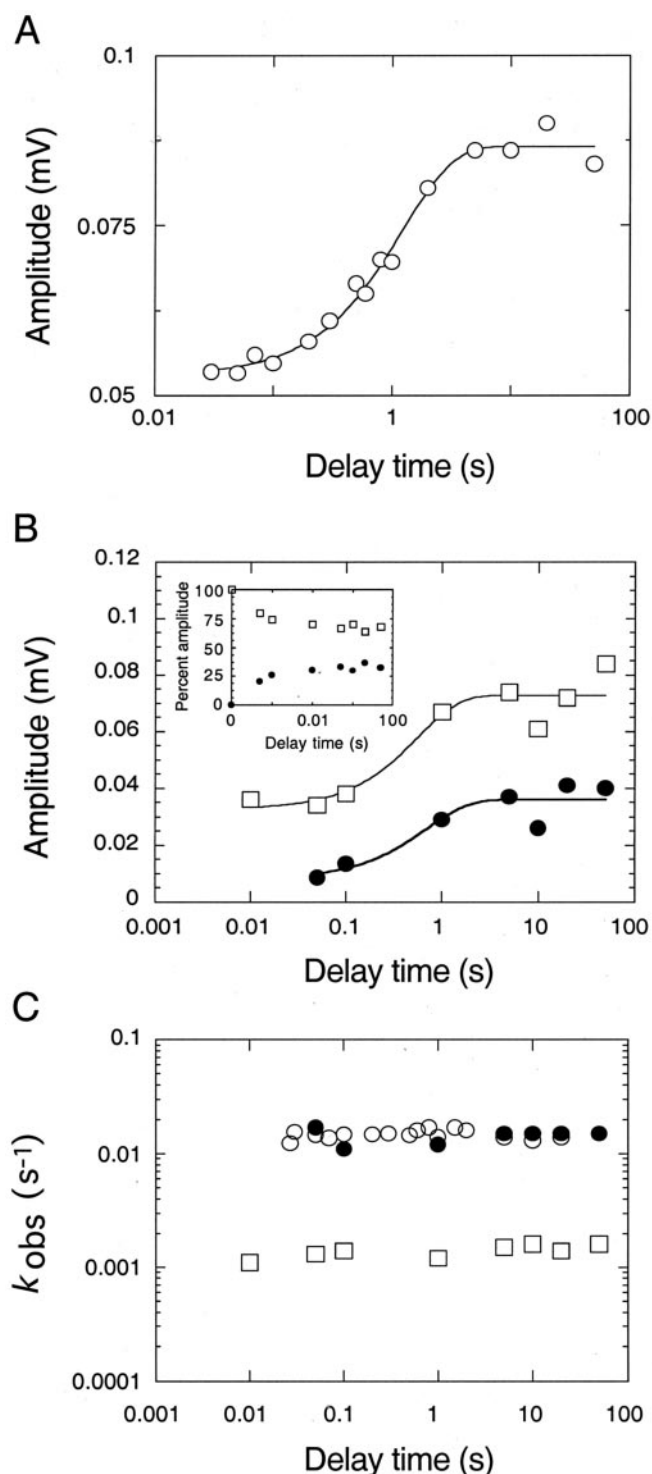
FIGURE 8. **Double-jump association-dissociation experiments.** After different delay times the complexes formed between 800 nM or 100 nM EBNA1$_{452-641}$ and 100 nM Site 1 5′-FAM were out-competed with 5 μM unlabeled Site 1. After the addition of unlabeled DNA, dissociation fluorescence traces were collected at different time-frames, and the data were fitted to exponential decays. *A*, corresponding amplitudes of the single phase obtained in excess of protein. The *line* represents the best fit of the data points to single exponential decay, yielding a rate of 0.8 s$^{-1}$. *B*, corresponding amplitudes of the two phases obtained in equimolar protein·DNA condition. The *lines* represent the best fit of the data points to single exponential decays, yielding rates of 1.4 s$^{-1}$ ($k_4$) (●) and 1.8 s$^{-1}$ ($k_3$) (□). *C*, recovered $k_{obs}$, of the phases obtained, in protein excess condition, 0.014 s$^{-1}$ ($k_{-1}^{DJ}$) (○), and in equimolar protein·DNA conditions, 0.014 s$^{-1}$ ($k_{-1}^{DJ}$) (●) and 0.0014 s$^{-1}$ ($k_{-2}^{DJ}$) (□).

mental conditions the $k_{obs}$ for complex formation was ~100 s$^{-1}$ (see Fig. 7C), which was faster than the dead-time of the double-jump experiment (10-ms delay time). Therefore, its disappearing amplitude was not observable. The progressive change of the amplitudes with the delay time is expected to be equivalent to the formation of the species in the "forward" direction. The increase in the single observed amplitude fitted to a single exponential (Fig. 8A) showed a rate of 0.8 s$^{-1}$ in agreement with the rate of the slow phase from pseudo-first order (2 s$^{-1}$, Fig. 7B), which we now identify as the rearrangement of the encounter complex to yield the consolidated complex.

The double-jump association-dissociation experiment was also carried out in equimolar protein·DNA concentration, equivalent to the pseudo-first order conditions of excess of DNA (not possible experimentally), where two association events were observed (Fig. 7C). After the longest delay time, where the signal is maximum, addition of excess unlabeled DNA yielded two phases of 0.014 s$^{-1}$ ($k_{-1}^{DJ}$) and 0.0014 s$^{-1}$ ($k_{-2}^{DJ}$) (Fig. 8C), and both rates were coincident with the dissociation rates observed by anisotropy and fluorescence of the consolidated complex (Fig. 5, *A* and *B*). The slowest dissociation rate ($t_{1/2} \sim 41$ min, Figs. 5A and 6A) was too slow to fit in the experimental window of a stopped-flow experiment.

The rates obtained from the amplitude change with delay time were 1.8 and 1.4 s$^{-1}$, $k_3$ and $k_4$, respectively (Fig. 8B). These rates were identical to the slow unimolecular rate observed in pseudo-first order, so they could not be discriminated in the forward direction but were only dissected in a double-jump experiment from their reverse reactions. The existence of both amplitudes from the earliest delay times indicates that they correspond to parallel rearrangement channels, and the fact that the percent amplitudes changed with time strongly suggests that they are connected, *i.e.* they can exchange. As the reaction progressed, the amplitudes stabilized at 65 and 35%, respectively (Fig. 8B, *inset*); however, we do not consider there should be a linear relationship between the fluorescence change and the actual percentage of the population.

Finally, under the experimental conditions for the association silent phase of the association-dissociation double-jump experiment (100 nM, 1:1 EBNA1·DNA), the association $k_{obs}$ was ~20 s$^{-1}$ ($t_{1/2}$ 35 ms). Considering a 10-ms dead-time for the delay mixing, one would have expected the amplitude corresponding to the encountered complex to disappear progressively, thus yielding the subsequent rearrangement described above. However, this phase did not yield any fluorescence change and could not, therefore, be followed due to experimental restrictions.

## DISCUSSION

The unusual topology of EBNA1 DNA binding "core" domain is shared with papillomavirus E2 DNA binding domain (Fig. 1). However, the recognition of the DNA in EBNA1 makes use of an additional domain, the "flanking" helical domain, with an extended chain that tunnels through the DNA helix as part of the specific contacts. The DNA binding helices in the core domain do not contact the DNA in the crystal structure, something that makes the DNA recognition mechanism rather puz-

zling (10), especially if one considers that the core domain displays binding activity and that mutations in the helix affect DNA binding (11). To address the basic binding mechanism to a minimum binding site, we carried out a detailed DNA binding analysis of EBNA1$_{452-641}$ in solution using various spectroscopic and biophysical methods. The stoichiometry was found to be 1:1 by different approaches, and a substantial conformational change in the DNA was observed in near-UV CD, in agreement with changes observed in the crystal structure of the complex (10). However, it is difficult to compare the magnitude of the change in solution with that in the crystal. Although the crystal provides atomic detail in a rigid conformation, the ellipticity change provides larger sensitivity in solution but lacks the possibility of assigning the changes precisely. In any case, a drastic change in one or more contiguous DNA sites is expected in this OBP, which prepares the origin for the action of the DNA helicase and replication machinery.

The binding affinity of EBNA1$_{452-641}$ to DNA in solution was 0.5 nM, which is in excellent agreement with that determined from EMSA, particularly considering the differences in the experimental conditions (11). The discrimination capacity ($K_{Dnon\text{-}specific}/K_{Dspecific}$) was determined to be ≥20,000, which is comparable to that of HPV16 E2C·DNA interaction with one of its specific sites: 10,000 (14).

Thermodynamic analysis of the interaction indicates that it is entirely enthalpically driven, which appears evident from the comparison of $\Delta G$ (measured by fluorescence spectroscopy) and $\Delta H$, and a negligible $\Delta S$. This also suggests that most of the enthalpic change comes from binding as opposed to local folding events, suggesting that the molecules behave as rigid bodies compared with other systems (26). The $\Delta C_p$ estimated from established algorithms using burial of surface area ($\Delta ASA$) values (27) is $-0.54$ kcal mol$^{-1}$ K$^{-1}$, compared with $-1.22$ kcal mol$^{-1}$ K$^{-1}$ for that determined experimentally in this work. This type of discrepancy is often found in protein-DNA interactions, because it is not as predictable as in protein folding reactions or in small molecules (28). On the other hand, the measured $\Delta C_p$ for the structurally homologous and functionally related E2 DNA binding domain from human papillomavirus is $-0.37$ kcal mol$^{-1}$ K$^{-1}$ (29), which shows little discrepancy with the predicted value, $-0.46$ kcal mol$^{-1}$ K$^{-1}$. The EBNA1$_{452-641}$·DNA complex buries 5,850 Å$^2$ against 3,544 Å$^2$ for the E2C·DNA counterpart. In addition, whereas 50% of the buried surface area in EBNA1$_{452-641}$·DNA complex formation is polar; this figure is 64% in the E2C·DNA complex, suggesting a less polar interface for EBNA1·DNA.

Although it is generally accepted that a large fraction of the $\Delta C_p$ is accounted by burial of surface area, there are several possible sources of $\Delta C_p$, and therefore, for the discrepancy between the "surface area only" empirical approach and the experimental data (30). The most obvious is a local or global folding process coupled to binding (24). The EBNA1 domain is very stable to chemical denaturation (11),[3] and this evidence limits a significant contribution by a coupled local, let alone global, folding process. Other possible sources are protonation

and ion binding events (31), but the EBNA1·DNA complex presents little effect of pH and salt concentration on the binding.[4] A recently described alternative explanation is the role of the network of water molecules at the interface, related in part to changes in soft vibrational modes of the trapped interface water molecules (30). With the present limited information, we are in favor of the latter interpretation, *i.e.* local changes in the cooperative network of interactions, possibly involving structural interfacial water molecules. This view agrees very well with a less polar interface in the EBNA1·DNA complex. Perhaps more polar interfaces provide better estimations for the algorithm.

The association reaction displays at least two major phases, one of them corresponding to an encounter complex taking place near the diffusion limit, comparable to the association rate of the HPV16 E2C domain and other systems (15, 32, 33). This species undergoes a conformational rearrangement to yield the final consolidated complex (15). An identical association phase is observed when monitoring changes in intrinsic tryptophan fluorescence, which is carried out in excess of DNA instead of protein, confirming there is one major association phase. Our interpretation is that the difference in the observed phases in either excess of protein or DNA comes from the presence of not unexpected protein conformers in solution, where in excess of protein, the fastest reacting protein conformer reacts preferentially, and a single phase was observed (Fig. 7*B*). On the other hand, in excess of DNA, there were plenty of these molecules to react with all EBNA1$_{452-641}$ species (at least two populations of conformers), and two phases were observed. The fact that the on-rates of these phases are separable supports conformationally distinct populations (Fig. 7*C*). The microheterogeneity of the protein may be potentially more extensive, but only two rates are distinguishable. In support for this, we observed heterogeneity in the EBNA1·DNA complex in EMSA experiments (Fig. 6*A*). Based on the unusual positioning of the major "binding helix" in the crystal structure of EBNA1·DNA and the presence of a flanking domain that travels through the DNA helix making base specific contacts, consecutive binding and rearrangement steps are the most likely explanation for this reaction pathway (11).

Three phases were observed for the dissociation reaction, in different time ranges, using different spectroscopic probes, experimental set-ups, and even a kinetic EMSA experiment. The best estimation of these rates are $k^{DJ}_{-1} = 0.014$ s$^{-1}$, $k^{DJ}_{-2} = 0.0014$ s$^{-1}$, and $k^r_{-3} = 0.00028$ s$^{-1}$, where the latter ($t_{1/2} \sim 41$ min) corresponds to the rate-limiting dissociation, because it agrees with that obtained in the EMSA experiment, a direct physical evidence of a slow dissociation, considering the large difference in experimental conditions. However, although the EMSA experiment cannot yield a large number of points to fit complex reactions, it does provide an accurate indication that, at the experimental dead time ($\sim 1$ min), 23% of the molecules have already dissociated (Fig. 6*B*). This is consistent with the fastest rate ($k^{DJ}_{-1}$, 0.014 s$^{-1}$).

When the double-jump experiments were carried out with excess of protein in the association stage (first mixing), a single

---

[3] C. Oddo, E. Freire, L. Frappier, and G. de Prat-Gay, unpublished results.

[4] C. Oddo and G. de Prat-Gay, unpublished results.
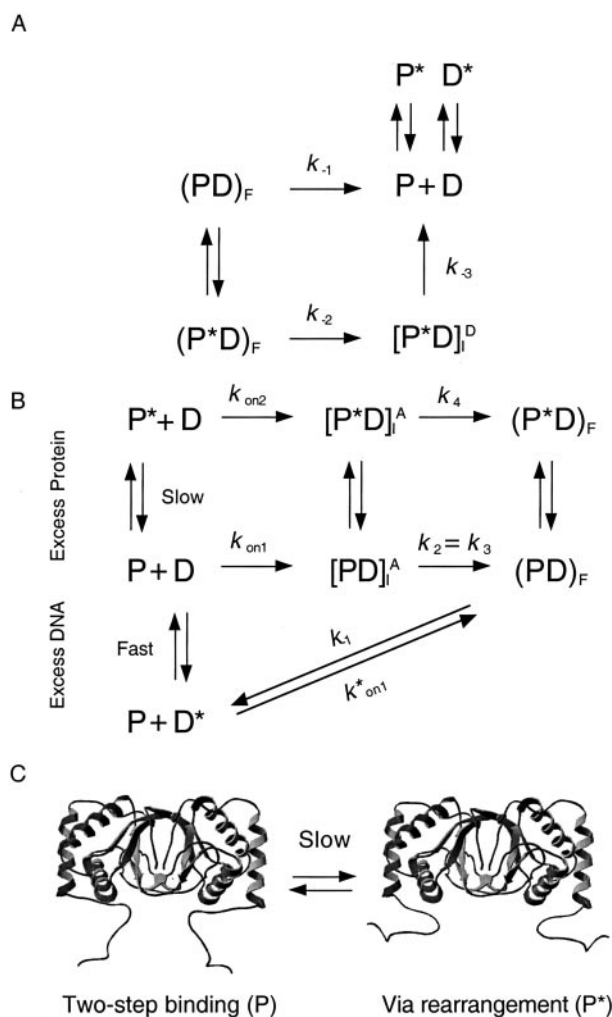
A

B

Excess Protein

Excess DNA

C



FIGURE 9. **A model for the origin site recognition mechanism by EBNA1$_{452-641}$.** *A*, dissociation showing two parallel routes. *B*, parallel association pathways in excess of protein or DNA and the two-step direct binding route. *C*, possible EBNA1$_{452-641}$ ensemble of conformers in solution: *P\**, species with disordered DNA-wrapping arm; *P*, species with ordered DNA-wrapping arm.

amplitude in the forward direction (Fig. 8*A*) corresponded to the rearrangement observed in the pseudo-first order experiment (~2 s$^{-1}$, Fig. 7*B*). An additional phase in the forward direction appeared in the analysis of the double-jump amplitudes when the complex was formed in equimolar concentrations (Fig. 8*B*), where both protein conformers could bind in parallel to DNA molecules. This additional forward phase, judging by the rate ($k_4$, 1.4 s$^{-1}$), would not be separable from the observed rearrangement in the forward direction even if it were accompanied by a strong fluorescence signal ($k_2$, 2 s$^{-1}$). Because it is not formed at the expense of the disappearance of $k_2$, we propose that this corresponds to the post-collision rearrangement of the parallel pathway, which not surprisingly appears similar to the single rearrangement directly observed in the forward reaction. Fig. 9 provides the simplest model for association and dissociation events that is compatible with the results presented here but in no way rules out other interpretations (Fig. 9, *A* and *B*).

We first focused on the dissociation because it is simpler to assign the rates and establishes the presence of two populations at the start of the reaction, which should be the product of the association reaction. The non-zero extrapolation establishes 23% of fast dissociating complexes, and this figure is very reliable because it does not involve an absolute fluorescence amplitude that may not be linearly related to the actual population of molecules but to the differential quantum yield of each species (Fig. 9). There is a parallel dissociation route, which corresponds to 77% of the complex molecules involving a dissociation intermediate, governed by the actual rate-limiting slow dissociation, observed both by spectroscopic (anisotropy and fluorescence) and direct (EMSA) measurements. In excess of protein, two parallel association events, as indicated by the early dissociation amplitudes observed in double-jump experiments, were observed, with two very similar on-rates ($k_{on1}^{W}$ and $k_{on2}^{W}$, $1.0 \times 10^8$ s$^{-1}$ M$^{-1}$ and $0.25 \times 10^8$ s$^{-1}$ M$^{-1}$, respectively) and rearrangement rates ($k_3 = 1.8$ s$^{-1}$ and $k_4 = 1.4$ s$^{-1}$, respectively). In excess of DNA, the heterogeneity could be explained by the presence of an additional protein conformer reacting with a preferential conformation of DNA. Conversely, in excess of protein, a preferentially reacting EBNA1$_{452-641}$ conformer appears to yield a single association event ($k_{on1}^{FAM} \approx k_{on1}^{W} = k_{on1}$, $1.6 \times 10^8$ s$^{-1}$ M$^{-1}$). However, the existence of a fast dissociation route in these conditions ($k_{-1}^{FAM} = 0.011$ s$^{-1}$) coincident with the early fast dissociating species from the double-jump experiment ($k_{-1}^{DJ} = 0.014$ s$^{-1}$ in excess of either protein or DNA) strongly suggests the presence of a parallel fast route, such as the one we described for the HPV E2·DNA complex (15). The collision events of direct and rearrangement mediated pathways are diffusion-controlled reactions and likely to display similar values. Therefore the $k_{-1}^{DJ}/k_{on1}^{FAM}$ ratio yields a value of 0.09–0.14 nM for the $K_D$, in excellent agreement with that determined from equilibrium experiments (0.5 nM, Fig. 3), supporting the existence of this direct fast route. We can hypothesize that the fast reacting EBNA1$_{452-641}$ conformer involved in the direct route is that containing an ordered "arm" domain (Fig. 9*C*, *left*). The route progressing through rearrangement will involve a population of EBNA1$_{452-641}$ conformers that bind through the core domain only (Fig. 9*C*, *right*) and require rearrangement at the interface to yield a consolidated complex. Overall, we pay more attention to the protein conformers, because the conformational heterogeneity of the DNA is likely to be greatly diminished in the context of the genome, as opposed to a small duplex, and is expected to be in fast exchange. Because the encounter need not discriminate base sequence, the complex formed in the two-state route, with a faster off-rate, may therefore need to undergo dissociation to re-bind to the specific target sequence while the intermediate encounter complex may slide along the DNA and find the correct sequence.

A possible mechanism, based on the crystal structure and mutagenesis, involves the interaction of the core domain followed by the interaction of the flanking domain with the DNA site (11). We have shown that such a mechanism is consistent with the results we present now, but further mutagenesis of the EBNA1$_{452-641}$ domain, in particular at the major core helices and the DNA-contacting arm, will be required to confirm the species involved in each step. In addition, NMR techniques in

solution will be required for a detailed structural and dynamic investigation of the protein·DNA complex.

## REFERENCES

1. McBride, A. A., Romanczuk, H., and Howley, P. M. (1991) *J. Biol. Chem.* **266,** 18411–18414
2. Klein, G. (1989) *Cell* **58,** 5–8
3. Yates, J. L., Warren, N., and Sugden, B. (1985) *Nature* **313,** 812–815
4. Reisman, D., and Sugden, B. (1986) *Mol. Cell. Biol.* **6,** 3838–3846
5. Sample, J., Henson, E. B., and Sample, C. (1992) *J. Virol.* **66,** 4654–4661
6. Jones, C. H., Hayward, S. D., and Rawlins, D. R. (1989) *J. Virol.* **63,** 101–110
7. Ambinder, R. F., Shah, W. A., Rawlins, D. R., Hayward, G. S., and Hayward, S. D. (1990) *J. Virol.* **64,** 2369–2379
8. Bochkarev, A., Barwell, J. A., Pfuetzner, R. A., Furey, W., Jr., Edwards, A. M., and Frappier, L. (1995) *Cell* **83,** 39–46
9. Hegde, R. S., and Androphy, E. J. (1998) *J. Mol. Biol.* **284,** 1479–1489
10. Bochkarev, A., Barwell, J. A., Pfuetzner, R. A., Bochkareva, E., Frappier, L., and Edwards, A. M. (1996) *Cell* **84,** 791–800
11. Cruickshank, J., Shire, K., Davidson, A. R., Edwards, A. M., and Frappier, L. (2000) *J. Biol. Chem.* **275,** 22273–22277
12. Summers, H., Barwell, J. A., Pfuetzner, R. A., Edwards, A. M., and Frappier, L. (1996) *J. Virol.* **70,** 1228–1231
13. Bochkarev, A., Bochkareva, E., Frappier, L., and Edwards, A. M. (1998) *J. Mol. Biol.* **284,** 1273–1278
14. Ferreiro, D. U., Lima, L. M., Nadra, A. D., Alonso, L. G., Goldbaum, F. A., and de Prat-Gay, G. (2000) *Biochemistry* **39,** 14692–14701
15. Ferreiro, D. U., and de Prat-Gay, G. (2003) *J. Mol. Biol.* **331,** 89–99
16. Ferreiro, D. U., Dellarole, M., Nadra, A. D., and de Prat-Gay, G. D. (2005) *J. Biol. Chem.* **280,** 32480–32484
17. Holowaty, M. N., Sheng, Y., Nguyen, T., Arrowsmith, C., and Frappier, L. (2003) *J. Biol. Chem.* **278,** 47753–47761
18. Frappier, L., and O'Donnell, M. (1991) *J. Biol. Chem.* **266,** 7819–7826
19. Barwell, J. A., Bochkarev, A., Pfuetzner, R. A., Tong, H., Yang, D. S., Frappier, L., and Edwards, A. M. (1995) *J. Biol. Chem.* **270,** 20556–20559
20. Gray, D. (1996) in *Circular Dichroism and the Conformational Analysis of Biomolecules* (Fasman, G., ed) pp. 469–499, Plenum Press, New York
21. Wiseman, T., Williston, S., Brandts, J. F., and Lin, L. N. (1989) *Anal. Biochem.* **179,** 131–137
22. Ladbury, J. E., and Chowdhry, B. Z. (1996) *Chem. Biol.* **3,** 791–801
23. Hegde, R. S. (2002) *Annu. Rev. Biophys. Biomol. Struct.* **31,** 343–360
24. Spolar, R. S., and Record, M. T., Jr. (1994) *Science* **263,** 777–784
25. de Prat Gay, G., Ruiz-Sanz, J., and Fersht, A. R. (1994) *Biochemistry* **33,** 7964–7970
26. Lundback, T., Chang, J. F., Phillips, K., Luisi, B., and Ladbury, J. E. (2000) *Biochemistry* **39,** 7570–7579
27. Tsodikov, O. V., Record, M. T., Jr., and Sergeev, Y. V. (2002) *J. Comput. Chem.* **23,** 600–609
28. Myers, J. K., Pace, C. N., and Scholtz, J. M. (1995) *Protein Sci.* **4,** 2138–2148
29. Di Pietro, S. M., Centeno, J. M., Cerutti, M. L., Lodeiro, M. F., Ferreiro, D. U., Alonso, L. G., Schwarz, F. P., Goldbaum, F. A., and de Prat-Gay, G. (2003) *Biochemistry* **42,** 6218–6227
30. Bergqvist, S., Williams, M. A., O'Brien, R., and Ladbury, J. E. (2004) *J. Mol. Biol.* **336,** 829–842
31. Kozlov, A. G., and Lohman, T. M. (1998) *J. Mol. Biol.* **278,** 999–1014
32. von Hippel, P. H., and Berg, O. G. (1989) *J. Biol. Chem.* **264,** 675–678
33. Winter, R. B., Berg, O. G., and von Hippel, P. H. (1981) *Biochemistry* **20,** 6961–6977
34. Hegde, R. S., Grossman, S. R., Laimins, L. A., and Sigler, P. B. (1992) *Nature* **359,** 505–512

# Mechanism of DNA Recognition at a Viral Replication Origin

Cristian Oddo, Eleonora Freire, Lori Frappier and Gonzalo de Prat-Gay

Access the most updated version of this article at doi: 10.1074/jbc.M602083200

Alerts:

- When this article is cited
- When a correction for this article is posted

Click here to choose from all of JBC's e-mail alerts

This article cites 33 references, 13 of which can be accessed free at
http://www.jbc.org/content/281/37/26893.full.html#ref-list-1